

Effects of tensor spin polarization on the chiral restoration and deconfinement phase transitions

Yan-Ru Bao¹ and Sheng-Qin Feng^{1, 2, 3, *}

¹*College of Science, China Three Gorges University, Yichang 443002, China*

²*Center for Astronomy and Space Sciences and Institute of Modern Physics,
China Three Gorges University, Yichang 443002, China*

³*Key Laboratory of Quark and Lepton Physics (MOE) and Institute of Particle Physics,
Central China Normal University, Wuhan 430079, China*

(Dated: March 26, 2024)

Abstract

Abstract: Effects of tensor spin polarization (TSP) on the chiral restoration and deconfinement phase transitions are studied in Polyakov loop extended Nambu-Jona-Lasinio (PNJL) model. For chiral phase transition, the higher the polarized degree of quark-antiquark pairs under the strong magnetic field, the higher the phase transition temperature. The TSP corrects the position of the critical end point (CEP). The small impact of TSP on the phase transition temperature is found for the deconfinement phase transition. On the other hand, we divide the phase space into three ranges based on the phase diagram obtained from the PNJL model: the confinement phase with chiral symmetry broken, the deconfinement phase with restored chiral symmetry, and the confinement phase with restored chiral symmetry (quarkonic phase). It is found that TSP has only a very small effect on the anisotropic pressure in the deconfined phase with chiral symmetry restored and the quarkyonic phase, but it has a very strong effect on the anisotropic pressure in the confined phase with chiral symmetry broken. This is because TSP is closely related to chiral symmetry. The restoration of chiral symmetry means the dissociation of spin polarization condensate.

* Corresponding author: fengsq@ctgu.edu.cn

I. INTRODUCTION

The properties of QCD matter under strong magnetic field background have attracted widespread interest among researchers [1–8]. In the early universe, the magnetic field may reach the order of 10^{22}G [9, 10]. The surface magnetic field of magnetars can reach 10^{14} – 10^{15}G , while its internal magnetic field can reach 10^{18} – 10^{20}G [11, 12]. And the extremely high magnetic fields can be generated in noncentral heavy ion collision experiments. The magnetic field created in RHIC experiments can reach $\sqrt{eB} \sim 0.1 \text{ GeV}$, while in LHC, the magnetic field intensity can reach $\sqrt{eB} \sim 0.5 \text{ GeV}$. Although the magnetic field is an external field with a short lifetime (of the order of $1 \text{ fm}/c$), the existence of quark-gluon plasma (QGP) medium response effect is significant, it greatly delays the decay of these time-dependent magnetic fields [13–16]. Therefore, it seems reasonable to assume the existence of a constant external magnetic field in many cases. The addition of strong magnetic field will make the phase diagram and phase structure of QCD more complex and interesting, leading to the emergence of many new phenomena, such as chiral magnetic effect (CME) [17–20], magnetic catalysis in vacuum (MC) [21–23], and inverse magnetic catalysis (IMC) [24–29] around chiral phase transitions.

The magnetic field also induces spin polarization, which is the condensate of quark antiquark pairs with parallel spins. As shown in reference [30], the tensor type interaction $(\bar{\psi}\Sigma^3\psi)^2 + (\bar{\psi}i\gamma^5\Sigma^3\psi)^2$ induces spin polarization $\langle \bar{\psi}i\gamma^1\gamma^2\psi \rangle$ which is analogous to the form of an anomalous magnetic moment (AMM) [30, 31] of quarks developed in the presence of a magnetic field. Note that the tensor polarization operator $\langle \bar{\psi}\sigma^{12}\psi \rangle$ is also known as the tensor spin polarization (TSP) operator or spin density, because $\langle \bar{\psi}\sigma^{12}\psi \rangle = \langle \psi^\dagger\gamma^0\Sigma^3\psi \rangle$ and with $\Sigma^3 = \begin{pmatrix} \sigma^3 & 0 \\ 0 & \sigma^3 \end{pmatrix}$, $\sigma^3 = -i\sigma^1\sigma^2$. By projecting the quark spinors ψ into the spin subspace $\psi = \psi_\uparrow + \psi_\downarrow$, one can obtain $\bar{\psi}\sigma^{12}\psi \sim \langle \bar{\psi}_\uparrow\psi_\uparrow \rangle - \langle \bar{\psi}_\downarrow\psi_\downarrow \rangle$, which measures the difference between spin up quark pairing and spin down quark pairing [7, 32].

The effects of TSP on the dynamic generation of quark magnetic moments in non-equilibrium quark matter, the magnetic properties of QCD matter, pion mass, and the chiral phase transition in the (2+1)-flavor Nambu-Jona-Lasinio (NJL) model have been investigated [7, 31, 32]. We know that the NJL model can only discuss issues such as chiral symmetry breaking and restoration phase transition, while the Polyakov loop extended Nambu-Jona-Lasinio (PNJL) model can analyze both chiral and deconfinement phase tran-

sition simultaneously.

In recent years, the anisotropy induced by magnetic fields has also been widely studied [33, 34]. The destruction of rotational symmetry by magnetic fields leads to the anisotropy of energy momentum tensors (EMTs). If the spatial elements of EMT are interpreted as the pressure generated by the response of the thermodynamic potential of the system to compression in the corresponding direction, there exists a difference caused by the orientation of the magnetic field in the local rest framework [35]. It has been proven that the derivative of the partition function obtained under constant magnetic flux corresponds to spatial elements where the directional difference of EMT becomes apparent. Usually, these different elements are referred to as longitudinal (P_{\parallel}) and transverse (P_{\perp}) pressures [26]. These quantities will affect the equation of state of strongly interacting substances.

Once the anisotropy of pressure under magnetic field background is considered, many studies on the equation of state (EOS) of dense stars will yield new results [35–47]. Due to the fact that both TSP and anisotropic pressure are caused by magnetic fields, it is of great research significance to focus on the influence of TSP on anisotropic pressure. In addition, under the magnetic field background, the original isotropic fermion vertices split into longitudinal and transverse fermions in the new tensor channel [28], and it is expected that this anisotropy will be reflected in pressure, and TSP will promote the anisotropy of pressure.

The impacts of TSP on the chiral restoration phase transition and deconfinement phase transition in the PNJL model are investigated in the paper. And then, the impacts of TSP on the anisotropic pressure under three different phase ranges are studied. This paper is organized as follows. The two flavor PNJL model with tensor channel is introduced in Sec. II. In Sec. III, we will study the distributions of TSP under different backgrounds, the influences of TSP on chiral restoration and deconfinement phase transition, and the effect of TSP on the anisotropy of pressure under three different phases. Finally, we make the summaries and conclusions in Sec. IV.

II. THE 2-FLAVORS PNJL MODEL WITH TSP

The destruction of rotational symmetry by uniform magnetic field leads to the separation of longitudinal and transverse-fermion modes along the direction of the magnetic field [28,

[30]. This separation leads to an effective splitting of the coupling in the gluon exchange interaction which the NJL model are usually based on. Therefore, this splitting can be reflected in the four-fermion coupling of the QCD effective field NJL model. By using Fierz identities [30, 32, 48] in a magnetic field, we can obtain the Lagrangian of the scalar and tensor interactions of the 2-flavor PNJL model as

$$\begin{aligned} \mathcal{L} = & \bar{\psi}(i\gamma^\mu D_\mu - m_0 + \gamma^0 \mu_q)\psi + G_s[(\bar{\psi}\psi)^2 + (\bar{\psi}i\gamma^5\psi)^2] \\ & + G_t[(\bar{\psi}\Sigma^3\psi)^2 + (\bar{\psi}i\gamma^5\Sigma^3\psi)^2] - \mathcal{U}(\Phi, \bar{\Phi}), \end{aligned} \quad (1)$$

where $\psi = (u, d)^T$ is two-flavor quark field with $\hat{m} = \text{diag}(m_u, m_d)$. Due to the spin symmetry of light quarks, the current quark mass is $m_0 = m_u = m_d$. $\Sigma^3 = \frac{i}{2}[\gamma^1, \gamma^2] = i\gamma^1\gamma^2$ is the spin operator. In addition, covariant derivative $D_\mu = \partial_\mu - iq_f A_\mu$ contains charge matrix $q_f = \text{diag}(q_u, q_d) = \text{diag}(\frac{2}{3}, -\frac{1}{3})$. In the external electromagnetic field $A_\mu = (0, 0, -Bx_1, 0)$, a constant and homogenous magnetic field of magnitude B points towards the x_3 -direction.

The second term in Eq. (1) is the traditional scalar channel, which produces a dynamical quark mass. The third term of Eq. (1) is the tensor channel, which preserves chiral symmetry and rotational symmetry along the direction of the magnetic field. Tensor channel is closely related to spin interactions, and induces spin polarization. In the magnetic field background, the running coupling constant is divided into longitudinal (g_\parallel) and transverse (g_\perp) components [30]. The coupling coefficients G_s and G_t of the NJL interaction related to quark gluon vertex coupling can be determined by $G_s = (g_\parallel^2 + g_\perp^2)/\Lambda^2$ and $G_t = (g_\parallel^2 - g_\perp^2)/\Lambda^2$. By setting $G_t/G_s = \alpha$, one can obtain $g_\parallel = g_\perp(\alpha = 0)$ at zero magnetic field, and $g_\parallel \gg g_\perp(\alpha \rightarrow 1)$ as $eB \rightarrow \infty$. In the following, we will choose the cases of $\alpha = 0$, $\alpha = 1/2$ and $\alpha = 1$.

By using the mean-field approximation, one can obtain the Lagrangian density as

$$\mathcal{L}_{MF} = \bar{\psi}(i\gamma^\mu D_\mu - M + \gamma^0 \mu_q - i\xi\gamma^1\gamma^2)\psi - \frac{\sigma^2}{4G_s} - \frac{\xi^2}{4G_t} - \mathcal{U}(\Phi, \bar{\Phi}), \quad (2)$$

where $M = m_0 + \sigma$ is the dynamical quark mass, and $\sigma = -2G_s \langle \bar{\psi}\psi \rangle$ is the chiral condensate. As mentioned earlier, tensor channels are closely related to spin-spin interactions. Under the background of a magnetic field, quark-antiquark pairs with opposite spin and opposite charge undergo orderly arrangement, resulting in tensor spin polarization condensate

$$\xi = -2G_t \langle \bar{\psi}\Sigma^3\psi \rangle. \quad (3)$$

The fourth term of Eq. (1) is the Polyakov potential $\mathcal{U}(\Phi, \bar{\Phi})$ associated with the deconfinement phase transition [49], where Φ is the order parameter describing the deconfinement

phase transition. When $\Phi \rightarrow 0$, the system is considered to be in the confinement phase, while when $\Phi \rightarrow 1$, the system is considered to be in the deconfinement phase. The Polyakov potential $\mathcal{U}(\Phi, \bar{\Phi})$ is given

$$\frac{\mathcal{U}(\Phi, \bar{\Phi})}{T^4} = -\frac{1}{2}A(T)\bar{\Phi}\Phi + B(T)\ln\{1 - 6\bar{\Phi}\Phi + 4(\bar{\Phi}^3 + \Phi^3) - 3(\bar{\Phi}\Phi)^2\}, \quad (4)$$

where the Polyakov potential $\mathcal{U}(\Phi, \bar{\Phi})$ is related to the Z(3) center symmetry. By simulating the deconfinement at finite temperature, one can obtain [50] the coefficients as

$$A(T) = a_0 + a_1\left(\frac{T_0}{T}\right) + a_2\left(\frac{T_0}{T}\right)^2, \quad (5)$$

$$B(T) = b_3\left(\frac{T_0}{T}\right)^3. \quad (6)$$

The different parameters [50] of Eq. (5) and Eq. (6) are given in Table I.

TABLE I. Parameters set for polyakov potential.

a_0	a_1	a_2	b_3	T_0 (MeV)
3.51	-2.47	15.2	-1.75	270

The effective potential at finite temperature and chemical potential obtained by the standardized process is

$$\begin{aligned} \Omega = & \frac{\sigma^2}{4G_s} + \frac{\xi^2}{4G_t} + \mathcal{U}(\Phi, \bar{\Phi}) - 3 \sum_{n,f,s} \frac{|q_f B|}{2\pi} \int_{-\infty}^{\infty} \frac{dp_z}{2\pi} \epsilon_{n,f,s} \\ & - T \sum_{n,f,s} \frac{|q_f B|}{2\pi} \int_{-\infty}^{\infty} \frac{dp_z}{2\pi} [T \ln(1 + g^-) + T \ln(1 + g^+)], \end{aligned} \quad (7)$$

where

$$g^-(\Phi, \bar{\Phi}) = 1 + 3(\Phi + \bar{\Phi} \exp\left(\frac{-E_{n,f,s}^{(-)}}{T}\right)) \exp\left(\frac{-E_{n,f,s}^{(-)}}{T}\right) + \exp\left(\frac{-3E_{n,f,s}^{(-)}}{T}\right), \quad (8)$$

$$g^+(\Phi, \bar{\Phi}) = 1 + 3(\bar{\Phi} + \Phi \exp\left(\frac{-E_{n,f,s}^{(+)}}{T}\right)) \exp\left(\frac{-E_{n,f,s}^{(+)}}{T}\right) + \exp\left(\frac{-3E_{n,f,s}^{(+)}}{T}\right), \quad (9)$$

where $E_{n,f,s}^{(\pm)} = \epsilon_{n,f,s} \pm \mu_q$, and dispersion relation of quarks with TSP [31, 32] is given by:

$$\epsilon_{n,f,s}^2 = \begin{cases} p_z^2 + (\sqrt{M^2 + 2n|q_f|B} - s\xi)^2, & n \geq 1, \\ p_z^2 + (M + \xi)^2, & n = 0, \end{cases} \quad (10)$$

where the summation of n is taken over all Landau levels. $f = u, d$ corresponds to flavor quantum number, and the $s = \pm 1$ corresponds to the different spin projections. Note that since the fermion in the lowest Landau level has only one spin projection, no splitting is present in the $n = 0$ case. But for the excited Landau levels $n \geq 1$, the spectrum of the quasi-quarks exhibits a Zeeman splitting ($s = \pm 1$) due to the tensor spin condensation ξ . One can obtain the gap equations as

$$\frac{\partial \Omega}{\partial M} = \frac{\partial \Omega}{\partial \xi} = \frac{\partial \Omega}{\partial \Phi} = \frac{\partial \Omega}{\partial \bar{\Phi}} = 0. \quad (11)$$

In order to ensure that the thermodynamic potential in vacuum is zero, we define the normalized thermodynamic potential as the effective potential [7]

$$\Omega_{eff}(T, \mu, eB) = \Omega(T, \mu, eB) - \Omega(0, 0, eB). \quad (12)$$

The expressions [33] of transverse pressure and longitudinal pressure are

$$P_{\parallel}(T, \mu, eB) = -\Omega_{eff}(T, \mu, eB), \quad (13)$$

$$P_{\perp}(T, \mu, eB) = P_{\parallel}(T, \mu, eB) - (\mathcal{M})eB, \quad (14)$$

where the magnetization $\mathcal{M} = -\frac{\partial \Omega_{eff}}{\partial (eB)}$.

It can be found that the energy integral term in the thermodynamic potential Eq. (7) is ultraviolet divergent. The renormalization scheme cannot be used to eliminate the divergence because of the dot-like interaction between quarks. Therefore, it is necessary to use appropriate regularization scheme to eliminate UV divergence. We use the Pauli-Villars regularization scheme with gauge covariance to eliminate the divergence in this paper. The key of Pauli-Villars regularization scheme is to replace integration with summation after introducing the normalized energy. The normalized energy is given [51] as

$$\epsilon_{n,f,s,i(PV)}^2 = \begin{cases} P_z^2 + (\sqrt{M^2 + 2n|q_f|B + a_i\Lambda^2} - s\xi)^2, n \geq 1, \\ P_z^2 + (\sqrt{M^2 + a_i\Lambda^2} + \xi)^2, n = 0, \end{cases} \quad (15)$$

$$\sum_{n,f,s} \int_{-\infty}^{\infty} \frac{dp_z}{2\pi} \epsilon_{n,f,s} \rightarrow \sum_{n,f,s} \int_{-\infty}^{\infty} \frac{dp_z}{2\pi} \sum_{i=0}^N c_i \epsilon_{n,f,s,i(PV)}, \quad (16)$$

the parameters of regularization scheme are given as $N=3$, $a_i = \{0, 1, 2, 3\}$ and $c_i = \{1, -3, 3, -1\}$. By fitting the vacuum values such as pion-decay constant $f_{\pi} = 93$ MeV and chiral condensation $\langle \bar{\psi}\psi \rangle = (-250 \text{ MeV})^3$, one can obtain [51] the relevant parameters such as $G_s = 3.44 \text{ GeV}^{-2}$, $\Lambda = 1127 \text{ MeV}$ and $m_0 = 5 \text{ MeV}$ at $G_t = 0$.

III. NUMERICAL RESULTS

A. Tensor spin polarization and chiral condensation

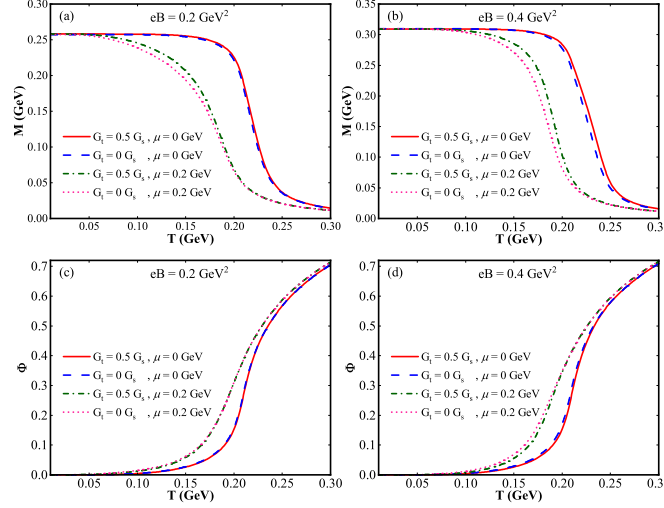


FIG. 1. The dynamical quark mass M and Polyakov loop Φ as functions of temperature T with different external magnetic field ($eB = 0.20 \text{ GeV}^2$ and $eB = 0.40 \text{ GeV}^2$) and different set of spin-spin interaction coupling constants ($G_t = 0 G_s$ and $G_t = 0.5 G_s$ for $\mu = 0 \text{ GeV}$ and $\mu = 0.20 \text{ GeV}$).

Firstly, we will investigate the effects of TSP on the chiral and deconfinement phase transitions. The temperature dependence of order parameters M and Φ under different magnetic fields and chemical potentials are shown in Fig. 1. As mentioned earlier, when G_t is zero, TSP contribution is zero, but when $G_t = 0.5 G_s$ is not zero, TSP contribution is not zero. The temperature dependences of chiral order parameters M in the case of $eB = 0.20 \text{ GeV}^2$ and $eB = 0.40 \text{ GeV}^2$ are manifested in Fig. 1(a) and Fig. 1(b). The chiral symmetry is broken with $M \neq 0$ at low temperature, and the chiral symmetry is restored with $M \rightarrow 0$ at high temperature. It is found that the chiral phase transition temperature increases by considering the influence of TSP. Comparing Fig. 1 (a) and Fig. 1 (b), we find that the increase of the phase transition temperature is more significant under higher magnetic fields ($eB = 0.40 \text{ GeV}^2$), which also means that the spin polarization effect is more significant under higher magnetic fields. The deconfinement phase transitions at $\mu = 0 \text{ GeV}$ and $\mu = 0.20 \text{ GeV}$ are shown in Fig. 1 (c) and Fig. 1 (d), respectively. It is found that the impact of TSP increases with the magnetic field, but slightly enhances the deconfinement

phase transition temperature.

In the $T - eB$ plane of Fig. 2, the corresponding temperature range is $0.01 \text{ GeV} \leq T \leq 0.25 \text{ GeV}$, and the magnetic field range is within $0.01 \text{ GeV}^2 \leq eB \leq 0.40 \text{ GeV}^2$. Figs. 2(a) and 2(b) display the contour plots of the spin polarization condensation $\xi = -2G_t \langle \bar{\psi} \Sigma^3 \psi \rangle$ with $\mu = 0 \text{ GeV}$ and $\mu = 0.20 \text{ GeV}$, respectively.

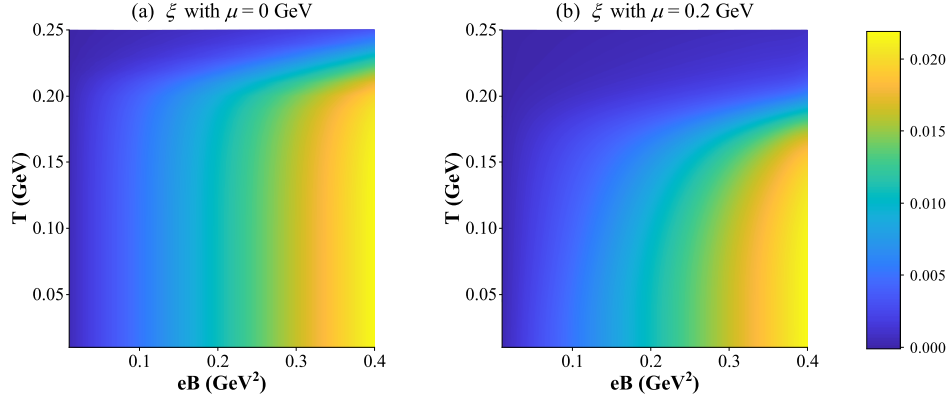


FIG. 2. (a), (b) show contour plots of the distribution of spin polarization condensate ξ for $\mu = 0 \text{ GeV}$ and $\mu = 0.20 \text{ GeV}$ in the $T - eB$ plane.

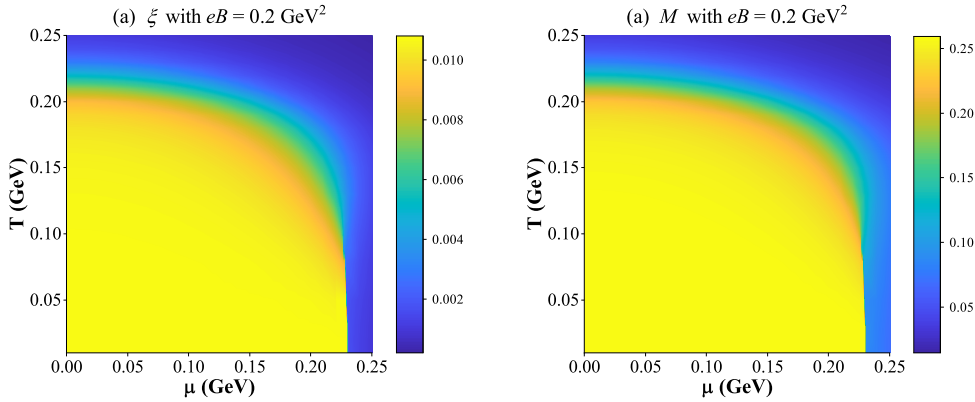


FIG. 3. (a), (b) show contour plots of the distribution of spin polarization condensate ξ and dynamical mass M for $eB = 0.20 \text{ GeV}^2$ in the $T - \mu$ plane.

The spin polarization condensate ξ decreases with the increase of temperature in the $T - eB$ plane shown in Fig. 2(a) and 2(b). This shows that the thermal background is not conducive to the formation of quark-antiquark pairs, which leads to the inhibition of TSP production. Fig. 2(a) - (b) show that ξ increases with the magnetic field under different

chemical potentials. this is because the charged quark-antiquark pairs are easier to be polarized under strong magnetic field.

Figure 3(a) and 3(b) show the distribution plots of spin polarization condensate ξ and dynamical quark mass M with $eB = 0.20 \text{ GeV}^2$ in the $T - \mu$ plane. It is worth noting that due to the close relationship between spin polarization condensate ξ (also called dynamical quark moment) and dynamical quark mass M [30, 31], the $T - \mu$ distribution diagrams of M and ξ are very similar. The distribution of ξ shows a continuous change at low chemical potentials and a sharp drop at high chemical potentials, which is consistent with the behavior of the order parameter M during chiral phase transition. Once quarks obtain a dynamical mass, they should also obtain a tensor spin polarization. This effect has also been reported in massless QED and in a one-flavor NJL model [30, 52, 53]. From the view of symmetry, once the chiral symmetry is dynamically broken, there is no symmetry protecting the TSP, because a nonvanishing value of the latter breaks exactly the same symmetry.

B. Phase diagram

The $T - \mu$ phase diagram of chiral and deconfinement phase transition with and without TSP ($G_t = 0 \text{ } G_s$ and $G_t = 0.5 \text{ } G_s$) under different magnetic fields are manifested in Fig. 4. It is found that the crossover occurs at high temperature and small chemical potentials μ while the first-order phase transition happens at low temperatures T and large chemical potential μ . The influences of TSP on the phase diagrams of the deconfinement phase transition and chiral phase transition can be summarized as follows: (1) In general, considering TSP, it has little effect on the deconfinement phase diagram, no matter whether it is a large magnetic field ($eB = 0.40 \text{ GeV}^2$) or a small magnetic field ($eB = 0.20 \text{ GeV}^2$). (2) TSP has great influence on the chiral phase diagram. In our chiral phase diagram, there is a crossover phase transition region and a first-order phase transition region. Considering the contribution of TSP, the influence on the first-order phase transition is larger and the influence on the crossover phase transition is smaller. However, with the increasing of magnetic field, the influence of TSP on the phase diagram will increase. When the magnetic field rises from 0.2 to 0.4 GeV^2 , the line of the first order phase transition line becomes longer as the magnetic fields become stronger. The results are consistent with those of Ref.[54].

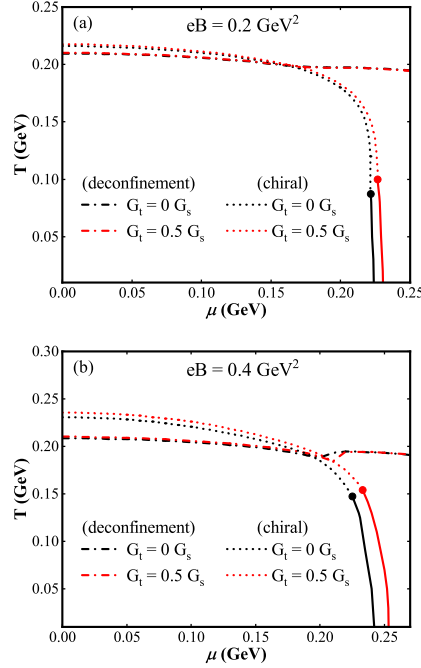


FIG. 4. $T - \mu$ phase diagram for chiral and deconfinement transition at different magnetic fields $eB = 0.20 \text{ GeV}^2$ and $eB = 0.40 \text{ GeV}^2$ for different spin polarization coupling constants $G_t = 0$ G_s and $G_t = 0.5 G_s$. The solid lines correspond to chiral first-order transition, the dash dot lines correspond to chiral crossover phase transition, the full dots correspond to CEP, and the dot lines correspond to deconfinement crossover phase transition.

In addition, according to the specific location of the critical end point (CEP) in Fig. 4, we list the location of the CEP in different cases in Table II. Compared with the case without TSP, we find that the introduction of TSP makes the position of CEP move slightly. The temperature and chemical potential of CEP are increased.

TABLE II. CEP position under different magnetic fields and spin polarization coupling constant G_t .

$eB = 0.20 \text{ GeV}^2$		$eB = 0.40 \text{ GeV}^2$
$G_t = 0 G_s$	$\{T_E, \mu_E\} = \{0.087, 0.222\}$	$\{T_E, \mu_E\} = \{0.148, 0.225\}$
$G_t = 0.5 G_s$	$\{T_E, \mu_E\} = \{0.102, 0.227\}$	$\{T_E, \mu_E\} = \{0.154, 0.233\}$

C. Anisotropic pressure

The phase diagrams of chiral phase transition and deconfinement phase transition using the PNJL model are shown in Fig. 4. According to this phase diagram, the phase space can be divided into three ranges: (1) The confinement phase with chiral symmetry broken, (2) The deconfinement phase with chiral symmetry restoration, (3) The confinement phase with chiral symmetry restoration (also known as quarkyonic phase). Next, we study the dependences of the normalized pressures P_{\parallel} and P_{\perp} on the magnetic field after the introduction of TSP in these three ranges, where P_{\parallel} is the pressure parallel to the magnetic field direction, and P_{\perp} is the pressure perpendicular to the magnetic field direction.

1. Anisotropic pressure in the confinement phase with chiral symmetry broken

By considering the influence of TSP, we study the dependence of the transverse pressure and longitudinal pressure on the magnetic field in the confinement phase with chiral symmetry broken in Fig. 5. Fig. 5(a) corresponds to $T = 0.15$ GeV, $\mu = 0.0$ GeV. The results show that at small magnetic field $eB = 0.01$ GeV², the transverse pressure and longitudinal pressure coincide. When $G_t = 0$, the spin polarization effect is not considered, P_{\parallel} and P_{\perp} almost do not change with the increase of the magnetic field, and P_{\parallel} and P_{\perp} are almost the same without splitting. When considering TSP ($G_t = 0.5 G_s$ and $G_t = G_s$), the longitudinal pressure P_{\parallel} increases not only with the increase of magnetic field, but also with the increase of G_t . While the transverse pressure P_{\perp} decreases not only with the increase of magnetic field, but also with the increase of G_t . That is to say, the splitting of P_{\parallel} and P_{\perp} not only with the increase of magnetic field, but also with the increase of G_t .

Fig. 5(b) corresponds to $T = 0.15$ GeV, $\mu = 0.10$ GeV, which is generally similar to that of Fig. 5(a). One finds that when $eB = 0.01$ GeV², the values of P_{\parallel} and P_{\perp} with $\mu = 0.10$ GeV are larger than that of $\mu = 0$ GeV, which is the natural result of more quark degrees of freedom [55]. On the other hand, it is surprising to find that when considering TSP, the transverse pressure P_{\perp} produces great oscillation with the increase of magnetic field.

Note that in the confinement phase with chiral symmetry broken, the influence of TSP on the longitudinal and transverse pressure is very significant. In conclusion, considering

the contribution of TSP increases the anisotropic characteristics of pressure in the magnetic field background.

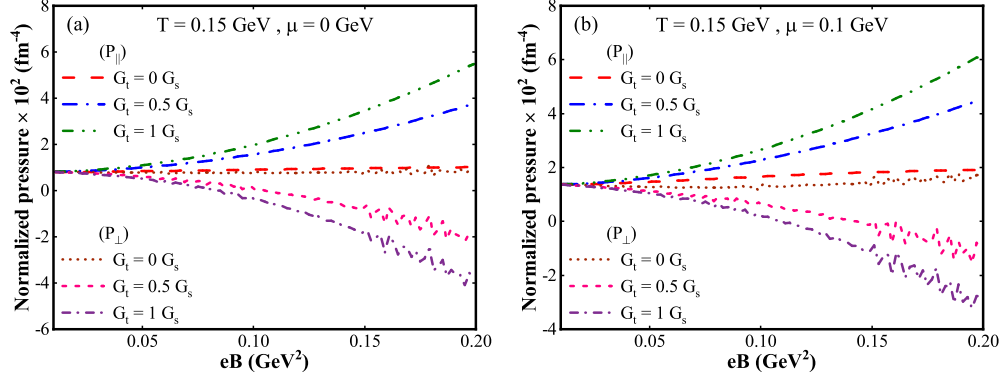


FIG. 5. Normalized longitudinal (P_{\parallel}) and transverse (P_{\perp}) pressure as a function of eB or the confinement phase with chiral symmetry broken for different spin polarization coupling constant G_t with different chemical potential $\mu = 0 \text{ GeV}$ (a) and $\mu = 0.2 \text{ GeV}$ (b), respectively.

2. Anisotropic pressure in the deconfinement phase with chiral symmetry restored

By considering the influence of TSP, we study the dependence of the transverse pressure P_{\perp} and longitudinal pressure P_{\parallel} on the magnetic field in the deconfinement phase with chiral symmetry restored shown in Fig. 6. It is found that the longitudinal pressure P_{\parallel} increases with the increase of the magnetic field, and transverse pressures P_{\perp} decrease with magnetic field. An obvious difference from the confinement phase with chiral symmetry broken is that the effect of TSP on anisotropic pressure is very small, and the effect of TSP can be almost ignored. With the restoration of chiral symmetry at high temperature $T = 0.25 \text{ GeV}$, the effect of TSP tends to zero.

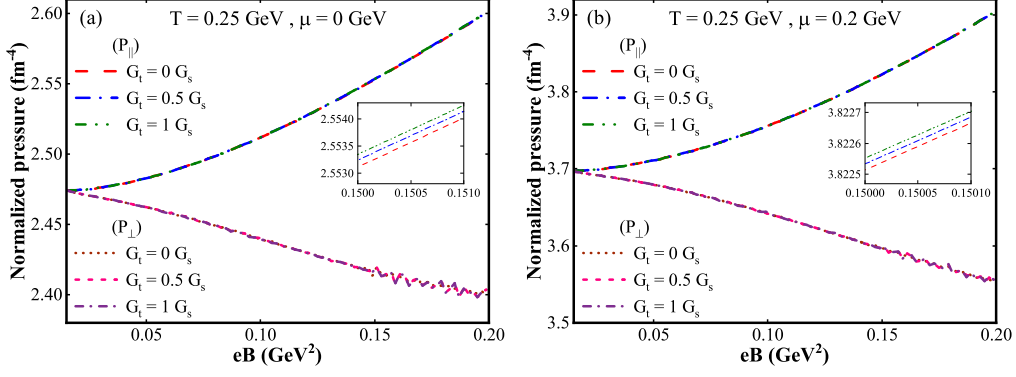


FIG. 6. Normalized longitudinal (P_{\parallel}) and transverse (P_{\perp}) pressure as a function of eB at deconfinement phase with restored chiral symmetry for different chemical potential $\mu = 0$ GeV (a) and $\mu = 0.2$ GeV (b), respectively.

3. Anisotropic pressure in the quarkyonic phase

Fig. 7 shows the dependences of longitudinal and transverse pressure on magnetic field in quarkyonic phase. Quarkyonic phase is a new phase of QCD, in which the chiral symmetry has been restored, but it is still in the confinement phase [33, 56–62]. When $T = 0.15$ GeV, $\mu = 0.35$ GeV, the dynamic quark mass is close to the current quark mass and $\Phi < 0.2$, which corresponds to the confinement phase with restored chiral symmetry, meaning that the system at quarkyonic phase. In this region, the effect of spin polarization condensate on the longitudinal and transverse pressures is very slight, similar to the deconfinement phase with restored chiral symmetry.

The results show that TSP has only a very small effect on the anisotropic pressure in the deconfined phase and the quarkyonic phase with chiral symmetry restored, but it has a very strong effect on the anisotropic pressure in the confined phase with chiral symmetry broken. This is also the result that TSP is closely related to chiral symmetry. The restoration of chiral symmetry means the dissociation of spin polarization condensate. Therefore, attention should be paid to the role of TSP in chiral symmetry breaking. TSP is closely related to the polarization caused by the magnetic field, and the pressure is also affected by the magnetic field. The pressures are slitted into the direction along the magnetic field and perpendicular to the magnetic field, which is a sign of anisotropy. Therefore, when

considering the anisotropy of pressure in chiral symmetry breaking phase, TSP will promote anisotropy.

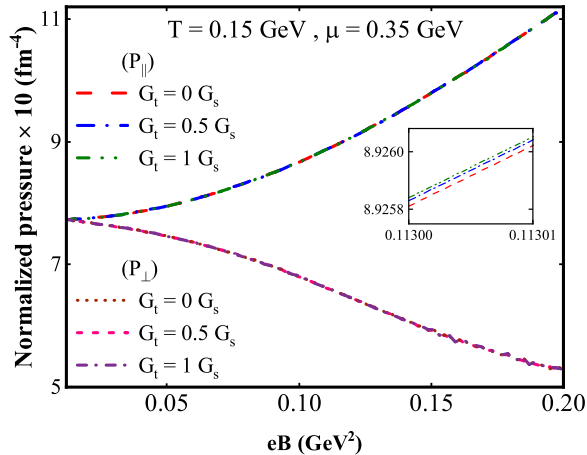


FIG. 7. Normalized longitudinal (P_{\parallel}) and transverse (P_{\perp}) pressure as a function of eB at quarkyonic phase.

IV. SUMMARY AND CONCLUSIONS

The generation mechanism of TSP is that quark and antiquark are polarized in the magnetic field background due to the opposite charge and spin, inducing a magnetic moment along the direction of the magnetic field. This new condensation formed by spin polarization interaction is called spin polarization condensate.

The introduction of TSP leads to an increase in the dynamical quark mass at the lowest Landau level in the magnetic field background, leading to an increase in the phase transition temperature. That is to say, for chiral phase transitions, the degree of polarization of quark-antiquark pairs increases with the magnetic field, resulting in an increase in the chiral phase transition temperature. The TSP will correct the position of the CEP. For the deconfinement phase transition, the effect of TSP on the phase transition temperature is very small, and it almost disappears at a large chemical potential.

Because the quark-antiquark pair produces magnetic moments along the direction of the magnetic field, the polarization of the quark-antiquark pair increases with the increase of the magnetic field, resulting in a larger TSP. In the high temperature QGP background, the pairing of quark and antiquark is blocked, and TSP decreases with the increase of

temperature and chemical potential. In addition, since the generation of TSP and chiral condensation depends on the pairing of quark and antiquark, the distribution of TSP is closely related to the chiral phase diagram. Under the same background, the phase transition temperature of TSP is basically the same as the chiral phase transition temperature.

It is found that TSP has only a very small effect on the anisotropic pressure in the deconfined phase with chiral symmetry restored and the quarkyonic phase, but it has a very strong effect on the anisotropic pressure in the confined phase with chiral symmetry broken. This is also the result that TSP is closely related to chiral symmetry. The restoration of chiral symmetry means the dissociation of spin polarization condensate. Therefore, attention should be paid to the role of TSP in chiral symmetry breaking.

ACKNOWLEDGMENTS

This work was supported by the National Natural Science Foundation of China (Grants No. 11875178, No. 11475068, No. 11747115).

REFERENCES

-
- [1] D. P. Menezes, M. B. Pinto, S. S. Avancini, A. P. Martinez, and C. Providencia, [Phys. Rev. C **79**, 035807 \(2009\)](#).
 - [2] V. A. Miransky and I. A. Shovkovy, [Phys. Rept. **576**, 1 \(2015\)](#).
 - [3] J. O. Andersen, W. R. Naylor, and A. Tranberg, [Rev. Mod. Phys. **88**, 025001 \(2016\)](#).
 - [4] X. G. Huang, [Rept. Prog. Phys. **79**, 076302 \(2016\)](#).
 - [5] D. E. Kharzeev, J. Liao, S. A. Voloshin, and G. Wang, [Prog. Part. Nucl. Phys. **88**, 1 \(2016\)](#).
 - [6] A. Bzdak, S. Esumi, V. Koch, J. Liao, M. Stephanov, and N. Xu, [Phys. Rept. **853**, 1 \(2020\)](#).
 - [7] Y.-W. Qiu and S.-Q. Feng, [Phys. Rev. D **107**, 076004 \(2023\)](#).
 - [8] Y.-W. Qiu, S.-Q. Feng, and X.-Q. Zhu, [Phys. Rev. D **108**, 116022 \(2023\)](#).
 - [9] M. Joyce and M. Shaposhnikov, [Phys. Rev. Lett. **79**, 1193 \(1997\)](#).
 - [10] A. Brandenburg, Y. He, T. Kahniashvili, M. Rheinhardt, and J. Schober, [Astrophys. J. **911**, 110 \(2021\)](#).

- [11] R. C. Duncan and C. Thompson, [Astrophys. J. **392**, L9 \(1992\)](#).
- [12] C. Thompson and R. C. Duncan, [Astrophys. J. **408**, 194 \(1993\)](#).
- [13] U. Grsoy, D. Kharzeev, and K. Rajagopal, [Phys. Rev. C **89**, 054905 \(2014\)](#).
- [14] X. Chen, S.-Q. Feng, Y.-F. Shi, and Y. Zhong, [Phys. Rev. D **97**, 066015 \(2018\)](#).
- [15] D. She, S.-Q. Feng, Y. Zhong, and Z.-B. Yin, [Eur. Phys. J. A **54**, 48 \(2018\)](#).
- [16] B.-X. Chen and S.-Q. Feng, [Chin. Phys. C **44**, 024104 \(2020\)](#).
- [17] K. Fukushima, D. E. Kharzeev, and H. J. Warringa, [Phys. Rev. D **78**, 074033 \(2008\)](#).
- [18] D. E. Kharzeev, L. D. McLerran, and H. J. Warringa, [Nucl. Phys. A **803**, 227 \(2008\)](#).
- [19] Y. Guo, S. Shi, S. Feng, and J. Liao, [Phys. Lett. B **798**, 134929 \(2019\)](#).
- [20] J. Deng and S.-Q. Feng, [Phys. Rev. D **105**, 026015 \(2022\)](#).
- [21] S. P. Klevansky and R. H. Lemmer, [Phys. Rev. D **39**, 3478 \(1989\)](#).
- [22] V. P. Gusynin, V. A. Miransky, and I. A. Shovkovy, [Nucl. Phys. B **462**, 249 \(1996\)](#).
- [23] V. P. Gusynin, V. A. Miransky, and I. A. Shovkovy, [Nucl. Phys. B **563**, 361 \(1999\)](#).
- [24] G. S. Bali, F. Bruckmann, G. Endr di, Z. Fodor, S. D. Katz, S. Krieg, A. Schfer, and K. K. Szab, [J. High Energy Phys. **2012**, 044 \(2012\)](#).
- [25] G. S. Bali, F. Bruckmann, G. Endr di, Z. Fodor, S. D. Katz, and A. Schfer, [Phys. Rev. D **86**, 071502 \(2012\)](#).
- [26] G. S. Bali, F. Bruckmann, G. Endr di, F. Gruber, and A. Schfer, [J. High Energy Phys. **2013**, 130 \(2013\)](#).
- [27] S. Fayazbakhsh and N. Sadooghi, [Phys. Rev. D **90**, 105030 \(2014\)](#).
- [28] M. Delia, F. Manigrasso, F. Negro, and F. Sanfilippo, [Phys. Rev. D **98**, 054509 \(2018\)](#).
- [29] S. Mao, [Phys. Rev. D **106**, 034018 \(2022\)](#).
- [30] E. J. Ferrer, V. de la Incera, I. Portillo, and M. Quiroz, [Phys. Rev. D **89**, 085034 \(2014\)](#).
- [31] S. Mao and D. H. Rischke, [Phys. Lett. B **792**, 149 \(2019\)](#).
- [32] F. Lin, K. Xu, and M. Huang, [Phys. Rev. D **106**, 016005 \(2022\)](#).
- [33] N. Chaudhuri, S. Ghosh, P. Roy, and S. Sarkar, [Phys. Rev. D **106**, 056020 \(2022\)](#).
- [34] K. Goswami, D. Sahu, J. Dey, R. Sahoo, and R. Stock, [arxiv , 2310.02711 \(2023\)](#).
- [35] D. Chatterjee, T. Elghozi, J. Novak, and M. Oertel, [Mon. Not. R. Astron. Soc. **447**, 3785 \(2015\)](#).
- [36] V. Canuto and H.-Y. Chiu, [Phys. Rev. **173**, 1210 \(1968\)](#).
- [37] A. P. Martnez, H. P. Rojas, and H. J. M. Cuesta, [Eur. Phys. J. C **29**, 111 \(2003\)](#).

- [38] J. L. Noronha and I. A. Shovkovy, [Phys. Rev. D **76**, 105030 \(2007\)](#).
- [39] E. J. Ferrer, V. de la Incera, J. P. Keith, I. Portillo, and P. L. Springsteen, [Phys. Rev. C **82**, 065802 \(2010\)](#).
- [40] X.-G. Huang, M. Huang, D. H. Rischke, and A. Sedrakian, [Phys. Rev. D **81**, 045015 \(2010\)](#).
- [41] M. Strickland, V. Dexheimer, and D. P. Menezes, [Phys. Rev. D **86**, 125032 \(2012\)](#).
- [42] M. Sinha, X.-G. Huang, and A. Sedrakian, [Phys. Rev. D **88**, 025008 \(2013\)](#).
- [43] E. J. Ferrer, V. de la Incera, D. M. Paret, A. P. Martinez, and A. Sanchez, [Phys. Rev. D **91**, 085041 \(2015\)](#).
- [44] D. P. Menezes, M. B. Pinto, and C. Providencia, [Phys. Rev. C **91**, 065205 \(2015\)](#).
- [45] D. P. Menezes and L. L. Lopes, [Eur. Phys. J. A **52**, 17 \(2016\)](#).
- [46] S. S. Avancini, V. Dexheimer, R. L. S. Farias, and V. S. Timteo, [Phys. Rev. C **97**, 035207 \(2018\)](#).
- [47] E. J. Ferrer and A. Hackebill, [Phys. Rev. C **99**, 065803 \(2019\)](#).
- [48] E. J. Ferrer, V. de la Incera, and X. . Wen, [Phys. Rev. D **91**, 054006 \(2015\)](#).
- [49] S. Rner, C. Ratti, and W. Weise, [Phys. Rev. D **75**, 034007 \(2007\)](#).
- [50] P. N. Meisinger, T. R. Miller, and M. C. Ogilvie, [Phys. Rev. D **65**, 034009 \(2002\)](#).
- [51] S. Mao, [Phys. Rev. D **99**, 056005 \(2019\)](#).
- [52] E. J. Ferrer and V. de la Incera, [Phys. Rev. Lett. **102**, 050402 \(2009\)](#).
- [53] E. J. Ferrer and V. de la Incera, [Nucl. Phys. B **824**, 217 \(2010\)](#).
- [54] P. J. de A. Bicudo, J. E. F. T. Ribeiro, and R. Fernandes, [Phys. Rev. C **59**, 1107 \(1999\)](#).
- [55] S.-Z. Su and X.-J. Wen, [J. Phys. G J. **48**, 075004 \(2021\)](#).
- [56] M. Abu-Shady, [Int. J. Theor. Phys. **54**, 1530 \(2014\)](#).
- [57] K. Fukushima, [Phys. Rev. D **77**, 114028 \(2008\)](#).
- [58] H. Abuki, R. Anglani, R. Gatto, G. Nardulli, and M. Ruggieri, [Phys. Rev. D **78**, 034034 \(2008\)](#).
- [59] F. Buisseret and G. Lacroix, [Phys. Rev. D **85**, 016009 \(2012\)](#).
- [60] N. Chaudhuri, S. Ghosh, S. Sarkar, and P. Roy, [Eur. Phys. J. A **56**, 213 \(2020\)](#).
- [61] Y. Hidaka, L. D. McLerran, and R. D. Pisarski, [Nucl. Phys. A **808**, 117 \(2008\)](#).
- [62] L. McLerran and R. D. Pisarski, [Nucl. Phys. A **796**, 83 \(2007\)](#).
- [63] L. McLerran, K. Redlich, and C. Sasaki, [Nucl. Phys. A **824**, 86 \(2009\)](#).